Heavy Neutral Leptons event selection at the ProtoDUNE experiment for NP04 LArTPC

CERN Summer Student Report 2025

Student:
Daniel Chalençon Maisian

Supervisor:
Animesh Chatterjee

European Center for Nuclear Research (CERN) - Neutrino Department - ProtoDUNE Experiment

July-August 2025

1 Introduction

ProtoDUNE is a large-scale neutrino experiment associated with the future Deep Underground Neutrino Experiment (DUNE), designed to validate Liquid Argon Time Projection Chamber (LArTPC) technologies. Located at CERN, it employes a 400 GeV proton beam from the Super Proton Synchrotron (SPS) to simulate neutrino interactions and study signatures of new physics. The experiment consists of two configurations: ProtoDUNE-DP (dual-phase) and ProtoDUNE-SP (single-phase, NP04), with the latter being the focus of this work.

This study focuses on the detection of Heavy Neutral Leptons (HNLs), hypothetical particles predicted by seesaw extensions of the Standard Model. HNLs provide a compelling solution to several open questions in particle physics and cosmology, including the origin of neutrino masses and the matter-antimatter asymmetry in the universe. ProtoDUNE's beamline and active detector volume allow probing HNLs at couplings significantly weaker than those accessible to previous experiments such as SHiP or NA62.

Thanks to its exceptional spatial and energy resolution, ProtoDUNE can effectively discriminate between HNL decay channels and background events. The primary objective of this work is to evaluate the sensitivity of ProtoDUNE-SP (NP04) to HNLs through Monte Carlo simulations of both signal and background processes.

The structure of this report is as follows: first, we present an overview of the ProtoDUNE-SP detector and its operational principles. Next, we discuss the phenomenology of HNLs within the detector environment. We then analyze background processes and perform a cut-based event selection to determine detection efficiencies. Finally, we summarize our findings and outline future prospects for enhancing the experiment's sensitivity to HNLs.

2 ProtoDUNE-SP NP04

The ProtoDUNE-SP detector was designed to validate the LArTPC technology in its single-phase configuration. It has two main purposes: to test detector performance (spatial and energy resolution) and to study hadronic/neutrino interactions as well as possible new physics signatures. At present, the detector is empty and aligned with the SPS beam.

The active volume measures 6 m in height (y-axis), 7 m along the drift direction (x-axis), and 7.2 m in depth (z-axis), making it the LArTPC with the longest drift distance (3.6 m) ever built. It also features the largest continuous drift volumes, each measuring 155.5 m^3.

Following a successful 10-week run, the detector underwent upgrades. It operates with a drift field of 500 V/cm across its anode plane assemblies (APAs) - three stacked wire planes enabling 3D track reconstruction through ionization signals - and contains approximately 800 tonnes of liquid argon. While stable operation is achieved at 180 kV, the voltage can be raised up to 300 kV. The upgrades include: a new cold electronics system (enhancing signal readout fidelity.), a new Photon Detector System (PDS) improving timing resolution for event reconstruction, and a cryostat maintaining a temperature of 87 K ($-186°$C), optimized for argon purity and stability. Future runs are foreseen, although challenges remain in trigger development to cope with high-rate beam conditions, as well as in event selection strategies for new physics searches.

The detector coordinate system is defined as follows: the z-axis is parallel to the beam-axis; the detector is offset downward from the beam centerline (y-axis) and centered in the drift coordinate (x-axis), as shown in figure 1a. The experimental setup consists of the SPS beam incident on a 50 cm thin beryllium (Be) target, producing numerous hadrons including $\pi^{\pm}$, $K^{\pm}$, η, π^0, ρ, and many others. Due to the momentum transfer from the protons, these hadrons become collimated along the beam direction and subsequently decay, producing neutrinos and, hypothetically, HNLs.

The reference frame takes the beam dump location as the origin. Neutrinos traversing the detector and scattering off argon nuclei can produce final states similar to those expected from HNL decays. For certain mass and coupling ranges where HNLs are long-lived, this makes ProtoDUNE-SP a lifetime frontier experiment, capable of probing unexplored regions of HNL sensitivity regions.

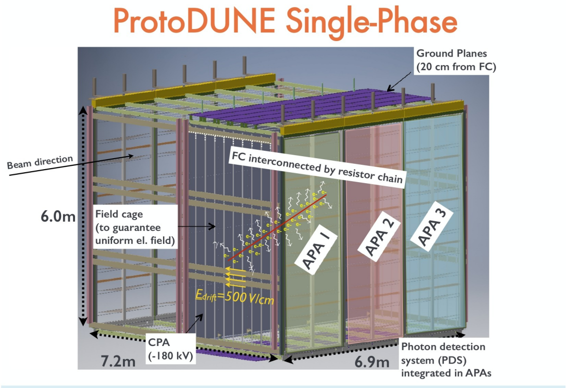

(a) Schematic of the ProtoDUNE-SP (NP04) detector showing dimensions and experimental setup. [1]

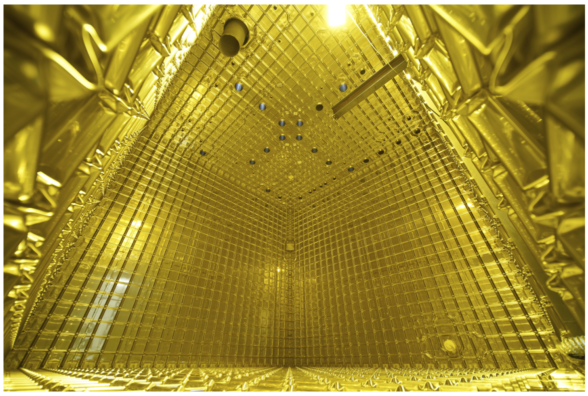

(b) Interior view of the ProtoDUNE-SP (NP04) cryostat prior to liquid argon filling.

Figure 1: The ProtoDUNE-SP NP04 detector.

3 Heavy Neutral Leptons phenomenology

In this section, we study the phenomenology of HNLs in the mass range from 10 to 500 MeV. The HNLs are produced at the target from hadronic interactions induced by the incident SPS beam, which generates a large number of hadrons. Their fluxes are simulated with **GEANT 4** and **Pythia**, and the used in **Madgraph** to simulate HNL production via meson decays. We assume a minimal type-I seesaw model with the inclusion of one HNL that mixes with active neutrinos through mixing parameters $U_{\alpha 4}$. Further details on the theoretical model can be found in [2].

For this study, we use truth-level simulation files (without detector reconstruction) generated with MadGraph 5. These correspond to couplings $|U_{e4}|^2$ and $|U_{\mu 4}|^2$ set to 10^{-6}, where the index "4" labels the HNL state. Detailed information on the simulation procedure, decay widths, normalization, and fluxes is provided in [3].

Table 1 summarizes the HNL production channels considered, restricted to pion and kaon decays.

In these decays, the N is highly boosted along the z-axis and can propagate over long distances, potentially reaching the detector depending on its mass and mixing. The probability that an HNL decays inside the detector is given by:

Coupling	$\pi^\pm$ decays	$K^\pm$ decays
$\|U_{e4}\|^2$	$\pi^\pm \to e^\pm N$	$K^\pm \to e^\pm N$ $K^\pm \to \pi^0 e^\pm N$
$\|U_{\mu 4}\|^2$	$\pi^\pm \to \mu^\pm N$	$K^\pm \to \mu^\pm N$ $K^\pm \to \pi^0 \mu^\pm N$

Table 1: Dominant HNL Production Channels from Pion and Kaon Decays

$$N_w = e^{-\Gamma_N L/\gamma\beta}\left(1 - e^{-\Gamma_N \Delta\ell_{det}/\gamma\beta}\right) \tag{3.1}$$

where L is the distance from the target to the detector, $\Delta\ell_{\text{det}}$ the detector length, and $\gamma\beta$ the boost factor of the HNL.

In the long-lived regime, i.e. in the limit $\Gamma_N L \ll \gamma\beta$, this probability can be approximated as:

$$N_w \approx \frac{\Gamma_N \Delta\ell_{det}}{\gamma\beta} \tag{3.2}$$

Table 2 summarizes the dominant HNL decay channels considered for the U_{e4} and $U_{\mu 4}$ couplings.

Coupling	Leptonic Decays	Semi-leptonic Decays
$\|U_{e4}\|^2$	$N \to e^\pm e^\mp \nu$ $N \to e^\pm \mu^\mp \nu$ $N \to \mu^\pm \mu^\mp \nu$	$N \to e^\pm \pi^\mp$
$\|U_{\mu 4}\|^2$	$N \to e^\pm e^\mp \nu$ $N \to e^\pm \mu^\mp \nu$ $N \to \mu^\pm \mu^\mp \nu$	$N \to \mu^\pm \pi^\mp$

Table 2: Dominant HNL Decay Channels for electron and muon couplings

It is worth noting that HNL production and decay channels also exist for the τ mixing, $U_{\tau 4}$, but are not considered in this work.

In the following, we study the kinematics of HNL decays by showing distributions of several relevant observables such as the energy and transverse momentum of the decay products. We also examine the HNL boost and the angular separation between leptons. These analyses are performed for different decay channels and several benchmark HNL masses.

U_{e4}

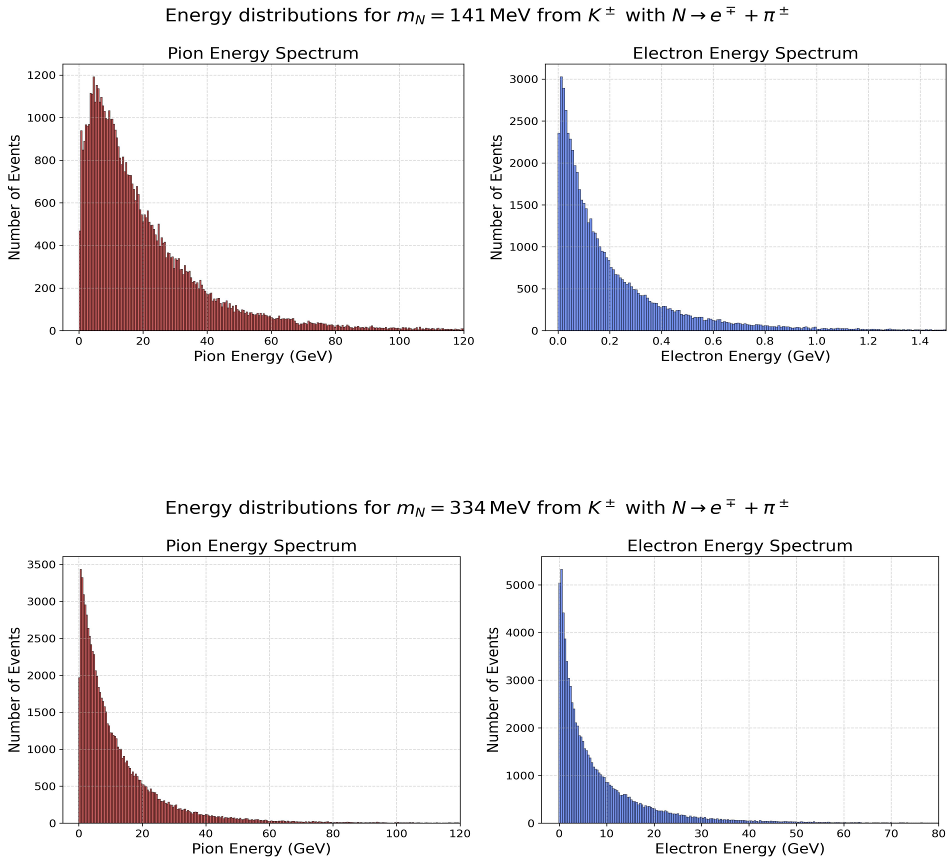

Figure 1: Energy distributions for $N \to e^{\pm}\pi^{\mp}$ decays at ($|U_{e4}|^2 = 10^{-6}$)

$U_{\mu 4}$

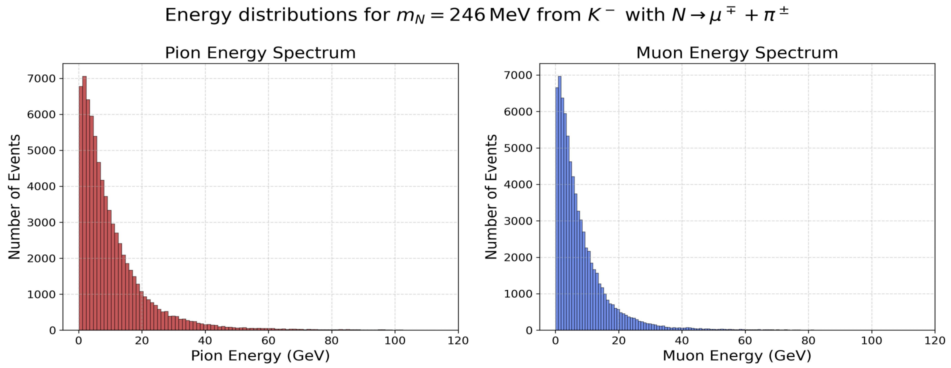

Figure 2: Energy distributions for $N \to \mu^{\pm}\pi^{\mp}$ decays at ($|U_{\mu 4}|^2 = 10^{-6}$)

$U_{e4}/U_{\mu 4}$

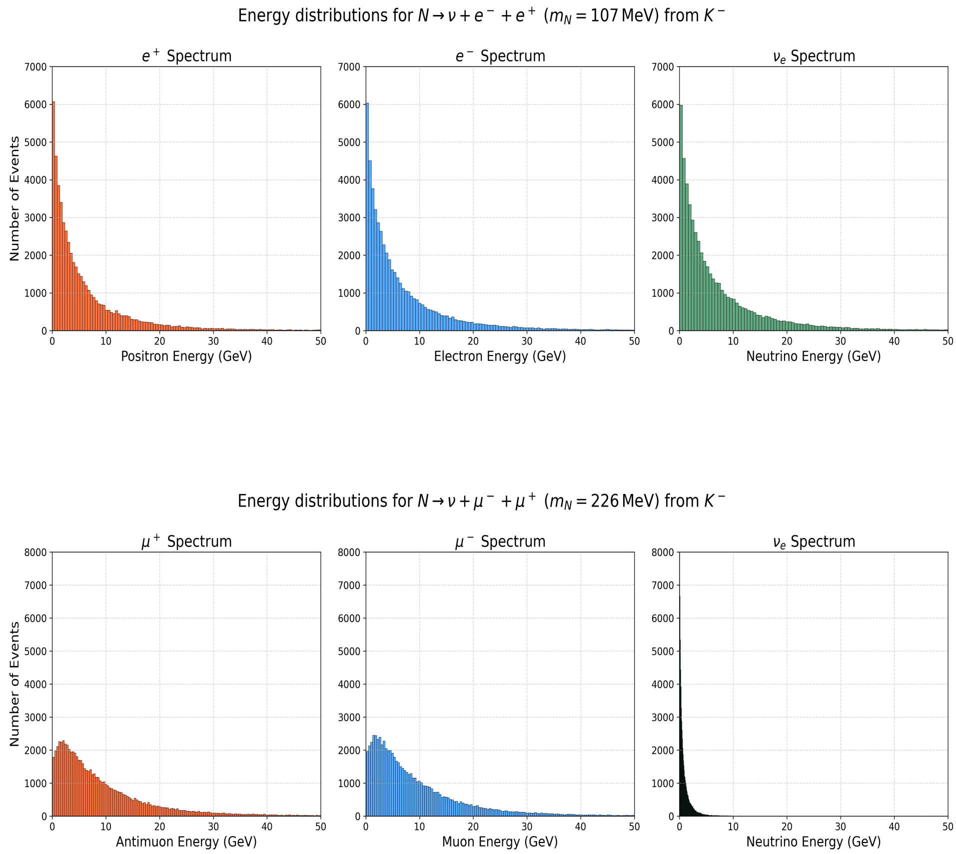

Figure 3: Energy distributions for $N \to \nu\, \mu^{\pm}\mu^{\mp}/N \to \nu\, e^{\pm}e^{\mp}$ decays at $(|U_{e4}|^2/|U_{\mu 4}|^2 = 10^{-6})$

The distribution of particle energies depends on the mass of the HNL and the identity of its decay products. The closer the mass of the daughter particle is to M_N, the larger the fraction of energy it carries. For instance, when M_N is close to m_π, almost all the available energy is transferred to the pion, while for higher HNL masses, when M_N moves further away from both m_π and m_μ, the energy distributions of the decay products become more balanced.

To avoid overloading the report, we do not display all transverse momentum distributions, as they generally lead to similar conclusions.

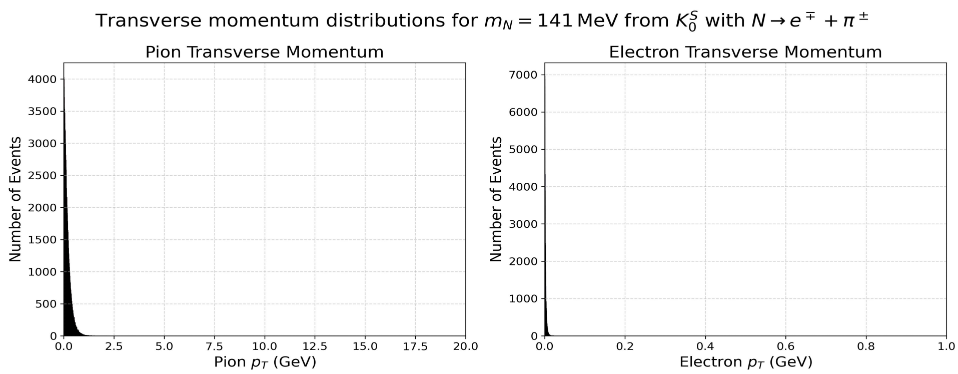

Figure 4: Transverse momentum distribution for $N \to e^{\pm}\pi^{\mp}$ decays at $(|U_{e4}|^2 = 10^{-6})$

The transverse momentum of the final-state particles is very low, since the decay products are highly collimated along the HNL flight direction. This feature is further reflected in the angular separation and boost distributions.

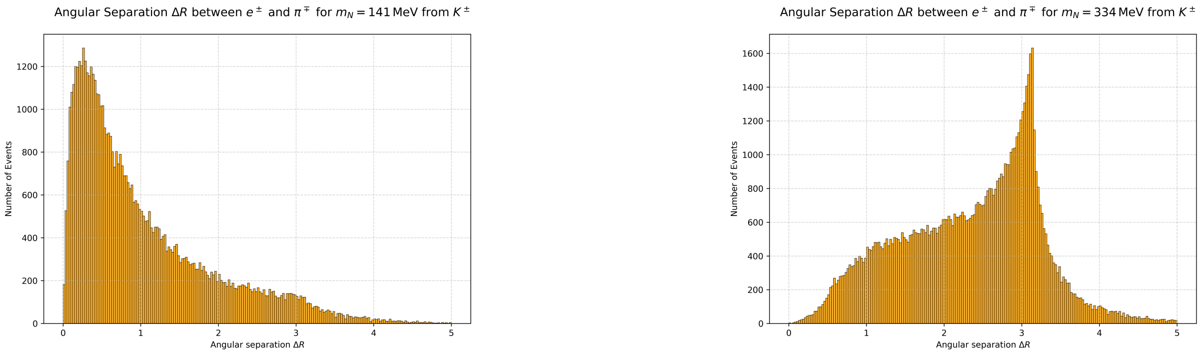

Figure 5: Angular separation distribution for $N \to e^{\pm}\pi^{\mp}$ decays at ($|U_{e4}|^2 = 10^{-6}$)

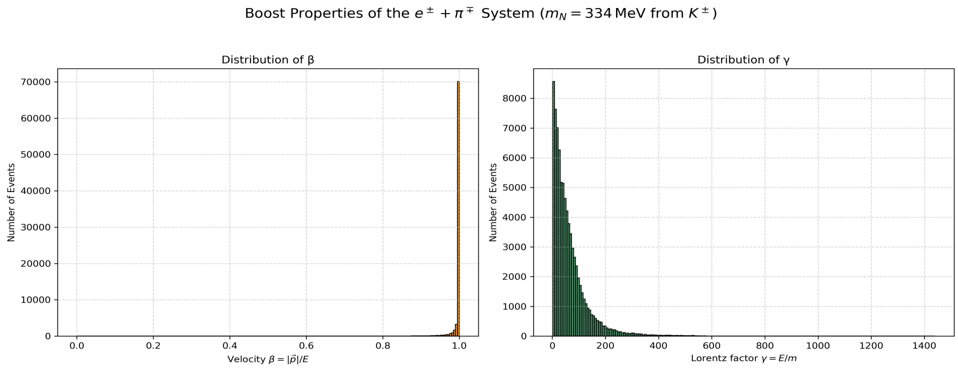

Figure 6: Boost parameters distribution for $N \to e^{\pm}\pi^{\mp}$ decays at ($|U_{e4}|^2 = 10^{-6}$)

From Fig. 5, we observe that for higher HNL masses, the angular separation between final-state particles increases, and the distribution becomes more uniform. As expected, three-body decays exhibit a broader angular spread than two-body decays, making them potentially easier to detect.

Furthermore, the invariant mass of the visible final states reconstructs a peak at the selected HNL mass, while the missing energy carried away by neutrinos in leptonic decays can be inferred from the deviation with respect to the total reconstructed energy.

It should be emphasized that these simulations are performed at truth level, i.e. without detector effects. As such, they do not exactly represent the measurable distributions in the experiment, but they provide a reliable overview of the underlying kinematics. In practice, neutrinos will escape detection, electrons and positrons will initiate electromagnetic showers, while muons and antimuons will leave charged tracks, though not necessarily depositing their full energy in the detector.

4 Background and event selection

In this section, we present the main background sources and perform a cut-based analysis aimed at maximizing the signal retention while suppressing background contamination.

To this end, we show the overlay of the energy and transverse momentum distributions, as well as the efficiency curves for the different decay channels at the chosen HNL benchmark mass points.

The background sources are the following:

- **Neutrino Interactions with Argon** (^{40}Ar):
  - **Charged Current (CC)**: $\nu_\ell + \text{Ar} \to \ell^- + \pi^\pm + X$
  - **Neutral Current (NC)**: $\nu_\ell + \text{Ar} \to \nu_\ell + \pi^0 + X$, with subsequent $\pi^0 \to \gamma\gamma \to e^+e^-$
- **Charm Production (DIS processes)**: $\nu_\ell + \text{Ar} \to \ell^- + D \to \ell^- + \ell'^+ + X$
- **Cosmics, rock interactions, and radioactivity**: These contributions are strongly reduced by applying timing, energy, and angular cuts.

In the following, we mainly focus on neutrino-induced events, which represent the most significant source of background. They are produced at the target and scatter on argon nuclei inside the detector, often mimicking the same final states as the signal, namely $\nu\, e^\pm e^\mp$, $\nu\, \mu^\pm \mu^\mp$, and $\nu\, e^\pm \mu^\mp$.

The neutrino events have been generated within the ProtoDUNE simulation chain: fluxes $\to$ GENIE $\to$ Geant4 $\to$ Pandora (see [4]). The output is stored in art-root files, which must be processed through an analyzer module in order to produce standard ROOT files containing the histograms and branches of interest.
A significant part of the work consisted in writing such an analyzer module in C++: it reads the available art-root files and creates branches that store all the particles produced in each event, assigning a unique identifier to each of them. Cuts are then applied on the energy, transverse momentum, and PDG codes of the particles/nuclei in order to keep only the relevant ones, while rejecting the numerous scattered nuclei and protons originating from secondary interactions. Invisible energy carriers, such as neutrinos produced in subsequent interactions, are also discarded.

In the following plots, we represent, as an example, the overlays of the E and p_T distributions at $M_N = 141$ MeV for the $e^\pm \pi^\mp$ decay channel. The y-axis represents the events fraction.

In figure 8, we have represented only two decay channels, $\nu\, e^\pm e^\mp$, and $e^\pm \pi^\mp$, as the last one shows the same distribution as the two others decay channels, namely $\nu\, e^\pm e^\mp$, and $\mu^\pm \pi^\mp$. We select between 4 and 8 HNL benchmark mass points for each decay channel considered and find the optimal cut in the energy that maximize the signal efficiency, while rejecting the more background possible. For each case, the optimal cut is defined as the cut value that maximizes the $S/\sqrt{S+B}$ curve, while retaining at least 35% of the signal and rejecting at least 50% of the background, as shown in figure 8. The optimal cuts and the associated efficiencies are summarized in Tables 3, 4, 5, and 6.

We observe that the best efficiencies are achieved at low energies for the $\nu\, e^\pm e^\mp$ decay channel. At high energies, the signal and background energy distributions are too similar for this process for any cut to be effective. In this channel, we cut the right side of the distribution, whereas in the three other channels, we cut the left and achieve consistently

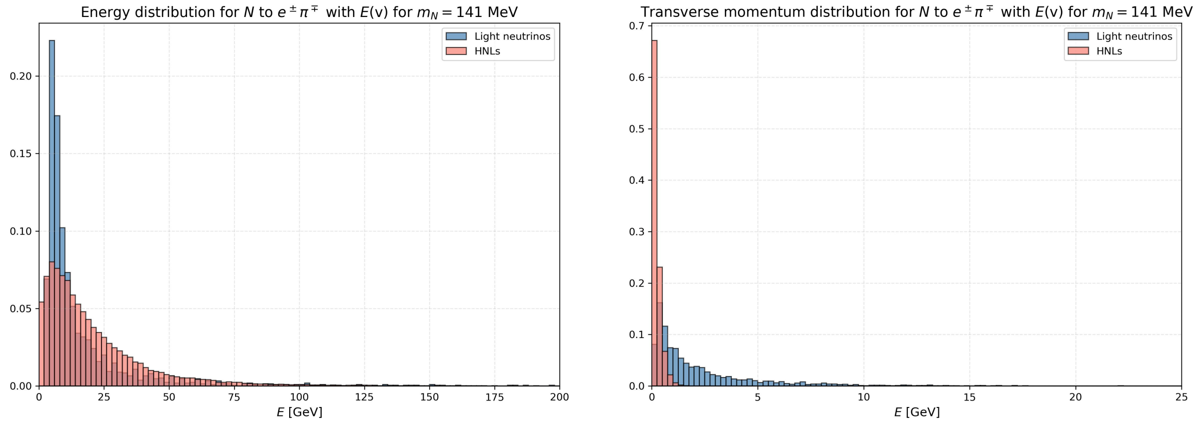

(a) Energy distribution (b) Transverse momentum distribution

Figure 7: Overlay of the energy and transverse momentum distributions for $M_N = 141$ MeV in the $e^{\pm}\pi^{\mp}$ decay channel.

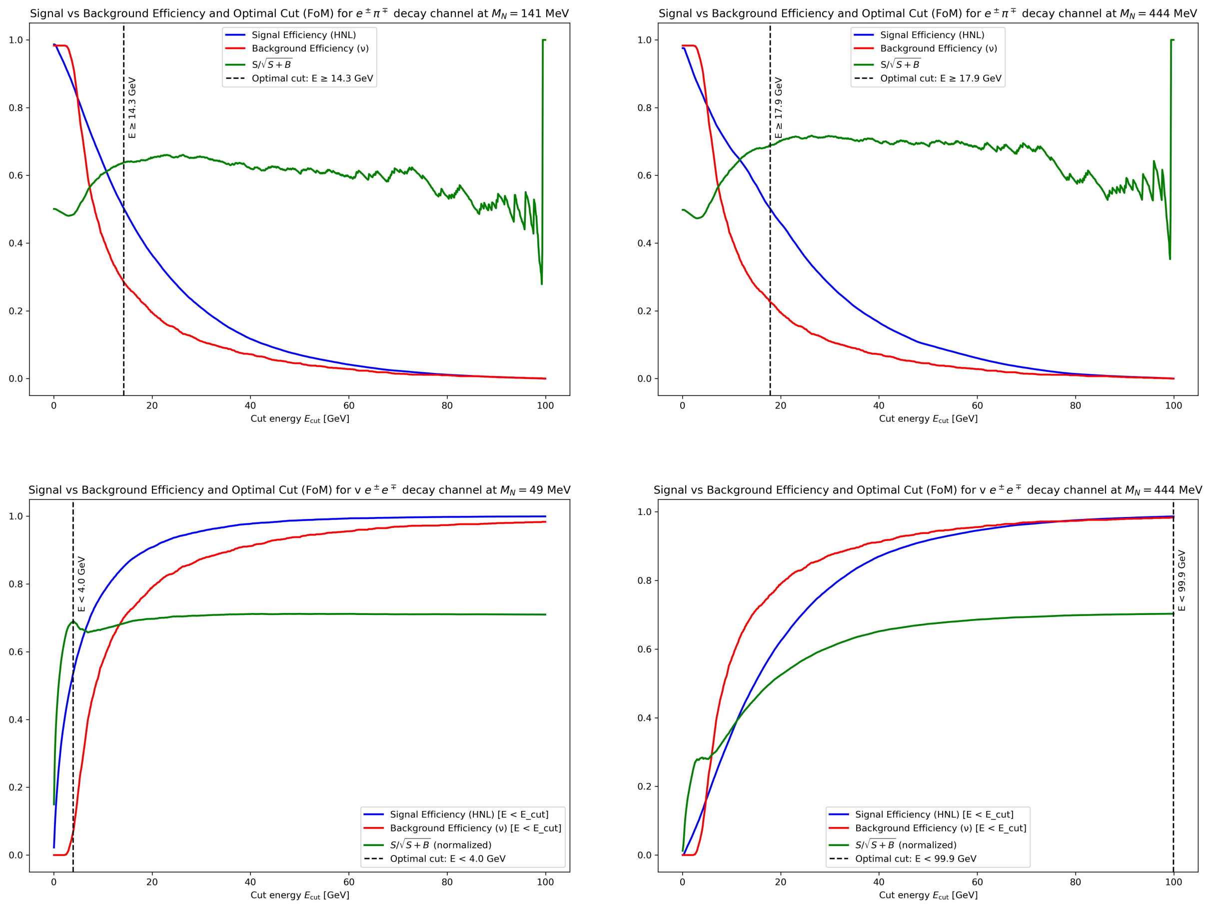

Figure 8: Efficiency curves for signal and background as a function of the cut energy, together with the $S/\sqrt{S+B}$ curve, and the optimal cut.

good efficiency across the entire mass range. Regarding the transverse momentum distributions, the signal and background are very similar, which implies that the optimal cut allows one to keep up to $85-95\%$ of the signal, while the background remains below 25%.

Mass	141	186	275	334	394	444	493
Sig. eff	51.30 %	51.12 %	51.32 %	51.62 %	52.72 %	52.39 %	55.29 %
Rem. Bkg	29.94 %	31.20 %	31.58 %	29.85 %	27.52 %	24.21 %	23.69 %
E cut (MeV)	≥ 14.3	≥ 13.8	≥ 13.6	≥ 14.4	≥ 15.7	≥ 17.9	≥ 18.3

Table 3: Table of the signal efficiency and remaining background fraction after applying the optimal cut for the process $N \to e^{\pm}\pi^{\mp}$

Mass	13	49	82	134	226	334	444
Sig. eff	56.32 %	53.60 %	38.04 %	99.40 %	99.52 %	99.47 %	99.04 %
Rem. Bkg	7.65 %	6.90 %	6.90 %	97.9 %	98.09 %	98.23 %	98.23 %
E cut (MeV)	≤ 4.1	≤ 4.0	≤ 4.0	≤ 90.0	≤ 95.6	≤ 99.1	≤ 99.1

Table 4: Table of the signal efficiency and remaining background fraction after applying the optimal cut for the process $N \to \nu\, e^{\pm}e^{\mp}$

Mass	226	275	334	394	444	493
Sig. eff	51.05 %	50.18 %	50.58 %	50.91 %	51.48 %	51.36 %
Rem. Bkg	33.12 %	35.82 %	37.08 %	35.40 %	33.12 %	31.30 %
E cut (MeV)	≥ 13.0	≥ 12.0	≥ 11.6	≥ 12.1	≥ 13.0	≥ 13.7

Table 5: Table of the signal efficiency and remaining background fraction after applying the optimal cut for the process $N \to \nu\, \mu^{\pm}\mu^{\mp}$

Mass	246	290	330	388
Sig. eff	51.12 %	50.99 %	51.62 %	55.48 %
Rem. Bkg	34.98 %	33.40 %	31.20 %	29.85 %
E cut (MeV)	≥ 12.3	≥ 12.9	≥ 13.8	≥ 14.4

Table 6: Table of the signal efficiency and remaining background fraction after applying the optimal cut for the process $N \to \mu^{\pm}\pi^{\mp}$

This behavior is mainly due to the fact that the HNL simulated events contain only two to three particles per event, which are highly collimated before their interaction inside the detector. In contrast, neutrino events typically contain between 80 and 150 particles per event, more diffusely distributed in the detector. The decay products of the HNLs have already interacted, releasing momentum in less collimated directions, which results in the transverse momentum distribution for neutrinos tending towards higher energies (see figure 7b). As a next step, it is necessary to access the reconstructed files. In comparison, our results and interpretations are in good agreement with those from the ICARUS study using the NuMI beam [5].

5 Conclusion and perspectives

In this work, we have intensively studied the kinematics of HNLs and active neutrino processes at high energy in the ProtoDUNE configuration. We developed an analyzer module in C++ to extract the relevant information from the simulation files and investigate the phenomenology of the decay channels, gaining experience with the LArSoft software and related tools.

We performed a cut-based analysis to prepare future sensitivity studies at the ProtoDUNE NP04 detector, achieving promising signal efficiencies, which nevertheless need to be further consolidated. In particular, it will be necessary to analyze the reconstructed HNL files in order to provide more realistic results, especially for the transverse momentum cuts at different energies and for the various decay channels. It will also be of great interest and provide complementary information to study the angles between leptons, as well as between showers, between tracks, and between showers and tracks at the reconstructed level. The next step is to quantify the sensitivity in terms of the background rejection and the achievable reach in the HNL mass–coupling parameter space. This will provide a more robust evaluation of the physics potential of ProtoDUNE in searches for HNLs.

References

[1] Laura Manenti. "ProtoDUNEs". In: *Prospects in Neutrino Physics*. May 2017. arXiv: `1705.05669 [physics.ins-det]`.

[2] Anupama Atre et al. "The Search for Heavy Majorana Neutrinos". In: *JHEP* 05 (2009), p. 030. DOI: `10.1088/1126-6708/2009/05/030`. arXiv: `0901.3589 [hep-ph]`.

[3] Josu Hernandez-Garcia. *Heavy Neutral Lepton Fluxes at DUNE Near Detector*. Tech. rep. Documentation technique, version 1.0. Institute for Theoretical Physics, ELTE Eötvös Loránd University, 2023. URL: `https://cernbox.cern.ch/index.php/s/QUfyw2rUHpyaDjy`.

[4] ProtoDUNE-BSM Collaboration. *pdhdbsmanalysis: Analysis framework for Heavy Neutral Leptons in ProtoDUNE*. `https://github.com/ProtoDUNE-BSM/pdhdbsmanalysis`. GitHub repository. 2025.

[5] Animesh Chatterjee, Josu Hernandez-Garcia, and Albert De Roeck. "Heavy Neutral Lepton searches at an ICARUS-like detector using NuMI beam". In: (Aug. 2024). DOI: `10.1140/epjc/s10052-025-13846-2`. arXiv: `2408.03383 [hep-ph]`.